



**HAL**  
open science

## An analysis of three-dimensional patterns of experimental detonation cells

Vianney Monnier, Vincent Rodriguez, Pierre Vidal, Ratiba Zitoun

► **To cite this version:**

Vianney Monnier, Vincent Rodriguez, Pierre Vidal, Ratiba Zitoun. An analysis of three-dimensional patterns of experimental detonation cells. 2022. hal-03632291v1

**HAL Id: hal-03632291**

**<https://hal.science/hal-03632291v1>**

Preprint submitted on 6 Apr 2022 (v1), last revised 14 Jun 2022 (v2)

**HAL** is a multi-disciplinary open access archive for the deposit and dissemination of scientific research documents, whether they are published or not. The documents may come from teaching and research institutions in France or abroad, or from public or private research centers.

L'archive ouverte pluridisciplinaire **HAL**, est destinée au dépôt et à la diffusion de documents scientifiques de niveau recherche, publiés ou non, émanant des établissements d'enseignement et de recherche français ou étrangers, des laboratoires publics ou privés.

# An analysis of three-dimensional patterns of experimental detonation cells

Vianney Monnier\*, Vincent Rodriguez, Pierre Vidal, Ratiba Zitoun

*Institut Pprime, UPR 3346 CNRS, Fluid, Thermal and Combustion Sciences Department,  
ENSMA, Téléport 2, 1 Av. Clément Ader, Chasseneuil-du-Poitou, 86360, France*

---

## Abstract

The notions of regularity and characteristic width of detonation cells are revisited based on crossed analyses of experimental head-on and longitudinal recordings obtained with the soot-plate technique. Tubes with cross-sections of different shapes, namely round, triangular and square, but the same surface area of  $16 \text{ cm}^2$ , are used to detonate the stable mixture  $2 \text{ H}_2 + \text{O}_2 + 2 \text{ Ar}$  at the initial temperature  $T_0 = 294 \text{ K}$  and the initial pressure  $p_0$  varying from  $15 \text{ kPa}$  to  $100 \text{ kPa}$ . The longitudinal recordings show the well-known regular arrangements for this mixture for all cross-section shapes and  $p_0$ , but those on the head-on recordings are irregular except for the square shape and low-enough  $p_0$ . There are fewer cells in the round tube, more in the square one, and their average widths and relative differences increase with decreasing  $p_0$ . All head-on cells become irregular and independent on the cross-section shapes with increasing  $p_0$ . In the square tube, the modulation of the cell phase shift suggests that randomly distributed phenomena with characteristic times at least the actual reaction time add up to compressibility, chemical kinetics and tube geometry. The cellular dynamics at the walls of a tube is thus not representative of that on the whole detonation front, and longitudinal soot traces alone are not sufficient for describing the cellular structure. An analysis based on elements of graph theory proposes that a tessellation of regular hexagons can model a large set of irregular head-on cells. This defines an average cell width from a cell count an experimental head-on recording and an intrinsic but high minimum error on the cell width. Its resulting oversensitivity to the parameters of the simplest Arrhenius rate of chemical evolution indicates that detailed schemes of chemical kinetics and more advanced conceptual tools than a single length are necessary for characterizing the three-dimensional patterns of detonation cells. The Voronoi tessellation supplemented with a physical criterion for the surface density of randomly-distributed point sources could represent a step forward.

---

\*Corresponding author: vianney.monnier@ensma.fr

## 1. Introduction

The instability of the reaction zones of self-sustained, e.g., Chapman-Jouguet (CJ), or overdriven detonation waves in gaseous mixtures was identified experimentally in the late 1950s by Denisov and Troshin [1], preceded by the observations of marginal detonations by Campbell and Woodhead [2]. Detonation fronts thus have a cellular structure, which is an impressive example of non-linearities in compressible reactive fluid dynamics such as those investigated by Clavin [3] for several varieties of reactive fronts. Higgins [4], Ng and Zhang [5], Vasil'ev [6], and Desbordes and Presles [7] reviewed experimental and numerical progress on detonation instability and cells. Understanding and characterizing this instability is useful for studying chemical kinetics in detonation reaction zones, calibrating numerical simulations and presizing safe industrial devices and advanced propulsion systems, e.g., [8–10].

To date, the cellular structure of the detonation is characterized based on representative lengths, namely the average width of the cells, e.g. [11], or the effective length of the reaction zone, that is, the Soloukhin's hydrodynamic thickness [12] further investigated by Lee and Radulescu [13, 14]. The increase in computational capabilities makes it possible to consider today predictable numerical simulations and other descriptions than characteristic lengths. This requires first collecting and analysing experimental data specific to the three-dimensional aspects of detonation cells, which is the object of this work.

A cellular reaction zone of detonation is an unsteady three-dimensional flow with unburnt and burnt gas pockets, and preceded by a leading shock made up of cells, that is, Mach waves with longitudinal and transverse fronts. Mach's method of traces on soot-coated plates is the usual technique to record geometrical information about cellular structure, e.g., [1, 15]. The typical setup is a straight detonation tube with the coated plates positioned longitudinally against its inner walls. The erosion of the coating by the transverse waves draws diamond-shaped patterns whose average width and regularity depend on the composition and the initial pressure and temperature of the mixture, or the transverse dimensions of the tube [16, 17]. This width is an usual characteristic length for characterizing the cellular structure. Values are available for many reactive mixtures [18] as functions of their equivalence ratio, dilution, initial pressure and temperature, e.g., [19–22], their confinements - such as straight or curved channels - and the detonation propagation mode - such as the steady propagation in tubes or transient dynamical conditions, e.g., transmission from a tube to a large volume or spherical expansion after direct ignition from a point source. The average width is accepted as a detonability indicator, that is, the capability of detonation to propagate in a system with finite transverse dimensions (another is the distance for the transition of deflagration to detonation, DDT). Thus, the smaller this width (or the DDT distance), the higher the detonability [23]. Shepherd et al. [24] and Zhao et al. [25] proposed automated methods to quantify cell width and irregularity using spectral and statistical analyses, respectively. More recently, Zhang et al. [26] reconstructed the cellular surface using the neural approach.

Cellular patterns on longitudinal soot foils have been categorized as very regular, regular, irregular and very irregular [16, 27], based essentially on recordings in square-section tubes. The average width of irregular patterns can thus be as large or even smaller than standard

deviation, raising questions on its representativeness [17]. Cell regularity is interpreted based on the chemical kinetics in the detonation reaction zone, e.g., [28–34]. Regular patterns are observed in mixtures with light fuels and oxygen highly diluted by a mono-atomic inert gas, typically argon, and irregular patterns in mixtures with heavier fuels and dilution with nitrogen [7]. Mixtures with regular or irregular patterns are also termed stable or unstable, respectively, e.g., [25, 35, 36]. Short [37] and Radulescu [38] carried out a modelling synthesis based on the Zel’dovich-Neuman-Döring (ZND) model of the detonation reaction zone. Irregularity corresponds with ZND induction zones large compared to reaction thicknesses. They proposed a regularity criterion based on the ratio of the former to the latter (the  $\chi$  number), the larger this ratio, the more unstable (irregular) the mixture. These interpretations thus involves chemical kinetics alone, whereas the shape of the cross-section of the detonation tube also determines how detonation cells behave. For example, regular mixtures show rectangular head-on cellular patterns only in tubes with rectangular cross-section, [39], and the marginal regimes of detonation propagation in regular mixtures are different depending on the cross-section shape. The usual control parameter for selecting marginal or multi-cellular detonation regimes in a given tube is the initial pressure because the larger it is, the smaller the cells.

There are only a few cells on the front of marginal detonations, and only one for the lower limit of propagation, e.g., [2, 40, 41]. For the round cross section, the limiting mode shows a spinning wave, that is, a single transverse wave rotating along the tube wall [42–45]. For the square cross section, the limiting mode shows two transverse waves normal to each other and reflecting on facing walls [42]. For slightly larger initial pressures, there can be two pairs of parallel transverse waves, each pair normal to the other and each wave of the same pair moving in opposite directions. The usual observation is the rectangular mode for which the transverse waves of a same pair are parallel to facing walls [46]. However, Hanana et al. [39, 47] identified a diagonal mode for which the transverse waves are angled by  $\pi/4$  to the tube walls, by passing the detonation through an obstacle with a square hole angled by  $\pi/4$  to the walls. Inductively, these experiments indicate that the three-dimensional properties of a cellular structure in a given mixture at given initial pressure and temperature depend on the dimension and the shape of the confinement [48] and, for marginal regimes, on the ignition method. Tsuboi et al. [49], Eto et al. [50], Deiterding [51], Wang et al. [52], Borisov and Kudryavtsev [53] and Taileb et al. [54] presented numerical simulations of rectangular and diagonal modes based on inviscid (Euler) equations coupled with either detailed chemical-kinetics or simple Arrhenius rates coupled with the constant- $\gamma$  equation of state. Williams et al. [55], Deledicque et al. [56] and Dou et al. [57] compared 2D and 3D numerical simulation of the one-cell rectangular mode and found the same cell width regardless of the dimensionality. In contrast, Takai et al [58] found the 2D cells smaller. The converse situation is that of cells small compared to the transverse dimensions of the tube or to the detonation size itself, e.g., the radius of a spherically expanding detonation. Although there are many observations and recordings of multi-cellular regimes of detonation, the 3D properties of a large set of such cells seem to have received less attention, apart from the indication by Takai et al. [59] that the volumes drawn by the transverse waves of rect-

angular modes are octahedrons and tetrahedrons. Therefore, 3D recording implementations should also investigate how the structure of multi-cellular fronts depends on the geometrical properties of the confinement, as suggested by Presles et al. [60].

Our work thus describes and analyses experiments in tubes whose cross sections have different shapes, namely square, triangular and cylindrical, based on head-on and longitudinal cell recordings on soot-coated foils for the regular mixture  $2\text{H}_2 + \text{O}_2 + 2\text{Ar}$ . This study is essentially experimental and descriptive, and intended only to discuss the cellular patterns, not to provide a predicting model for their sizes. Section 2 details the setups and their instrumentation, Section 3 presents the experimental results, Section 4 investigates how elements of graph theory can help interpret these results, and Section 5 discusses and concludes the work.

## 2. Methodology and experimental setup

We carried out a series of recordings in tubes with round (R), equilateral triangular (T) and square (Q) cross sections of the same area to within  $\pm 4\%$ . We also carried out some recordings in round and square tubes with larger cross sections (R' and Q' resp.). Table 1 shows the inner dimensions of the tubes.

Tube	Cross-section area (cm <sup>2</sup> )	Diameter or side length (mm)	Length (m)
R	16.6	46	6
T	16.1	61	1
Q	16.0	40	6
R'	70.8	95	10
Q'	25.0	50	6

Table 1: Dimensions of the tubes. R,R': round, T: equilateral triangle, Q,Q': square

We selected the stoichiometric reactive mixture  $2\text{H}_2 + \text{O}_2 + 2\text{Ar}$  because its regular cellular pattern in Q tubes at low-enough initial pressures (Section 1) is a convenient reference for comparison with the patterns in the R and T tubes. The mixture was prepared in a separate tank using the partial-pressure method, and then injected at the desired initial pressure  $p_0$  after vacuuming the tubes. We varied the initial pressure  $p_0$  from 15 kPa to 100 kPa and the initial temperature was  $294 \pm 3$  K for all experiments.

Figure 1 shows the schematic of an R or a Q tube. A spark plug or an exploding wire was used for ignition; Shchelkin spirals then ensured the transition to detonation on a very short distance, typically 1 m. Longitudinal and head-on recordings of the cellular structure were obtained using soot-coated foils positioned at the end of the tubes opposite to ignition. The longitudinal soot foils were 50-cm long and 1-mm thick. They were shaped into a half-cylinder for the R tubes, and a plate for the Q tubes.

The T tube was 1-m long. It was inserted at the end opposite to ignition in the 10-m long R' tube (Table 1) so that the detonation be steady before entering the T tube. Its three

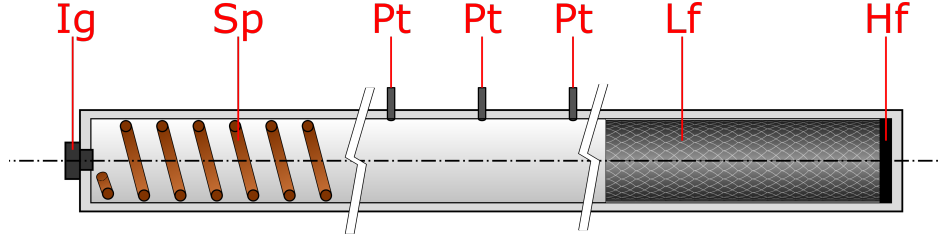


Figure 1: Schematic of a round (R) or square (Q) tube. Ig: ignition, Sp: Shchelkin spiral, Pt: pressure transducers, Lf: longitudinal soot foil, Hf: head-on soot foil

inner faces were coated with soot over their whole length before being assembled in such a way as to ensure sharp and equal inner angles.

Three Kistler 603B pressure transducers coupled with Kistler 5018A electrostatic charge amplifiers were positioned on the R and Q tubes before their soot-foil section. The triggering of the transducers was used to obtain the average velocity of the detonation wave and check its steadiness in the soot-foil section. Steadiness was also checked from the longitudinal recordings that showed cells with geometrical properties constant from the beginning to the end of each soot foil. There was no transducers on the T tube. Steadiness in this case was deduced only from the soot recordings. Similarly to those in the R and Q tubes, they showed cells with constant properties, except for a few centimeters of adaptation at the T-tube entry.

### 3. Results

#### 3.1. Cell patterns and cross-section shapes and areas

Figures 2 to 5 show typical head-on and longitudinal soot recordings.

At lower initial pressures, from  $p_0 = 15$  to 20.0 kPa (Figures 2 to 4, respectively), the head-on recordings in the Q tube show the long-time identified regular arrangement of square and rectangular patterns whose distributions depend on the instant of the detonation impact. These distributions are analyzed in subsection 3.2. However, the arrangements in the T and R tubes are stochastic, and repeated experiments show no dependency on the instant of impact. Although counting is difficult, a detonation front in an R tube appears to contain fewer cells than in the T and Q tubes, and in the T tube than in the Q tube, for the same  $p_0$ . The longitudinal soot recordings shows cells more irregular in the T and R tubes than in the Q tube, and slimmer in the Q tube than in the T and R tubes. In the Q tube, they also show a regular spacing of the reflection impacts of the transverse fronts moving parallel to the longitudinal plate.

At intermediate initial pressures, from 20.0 to about 70.0 kPa (Figures 5 and 6, respectively), the rectangular patterns on the head-on recordings in the Q tube are locally deformed with complex shapes similar to those on the T and R head-on recordings. The deformation domains have a stochastic distribution and spread with increasing  $p_0$ , although the longitudinal recordings in the Q tube still show a regular spacing of the transverse impacts.

At higher initial pressures, from  $p_0 \geq 70$  kPa (Fig. 6), the deformation domains eventually covers the whole section of the Q tube. There is no transverse waves moving parallel to the

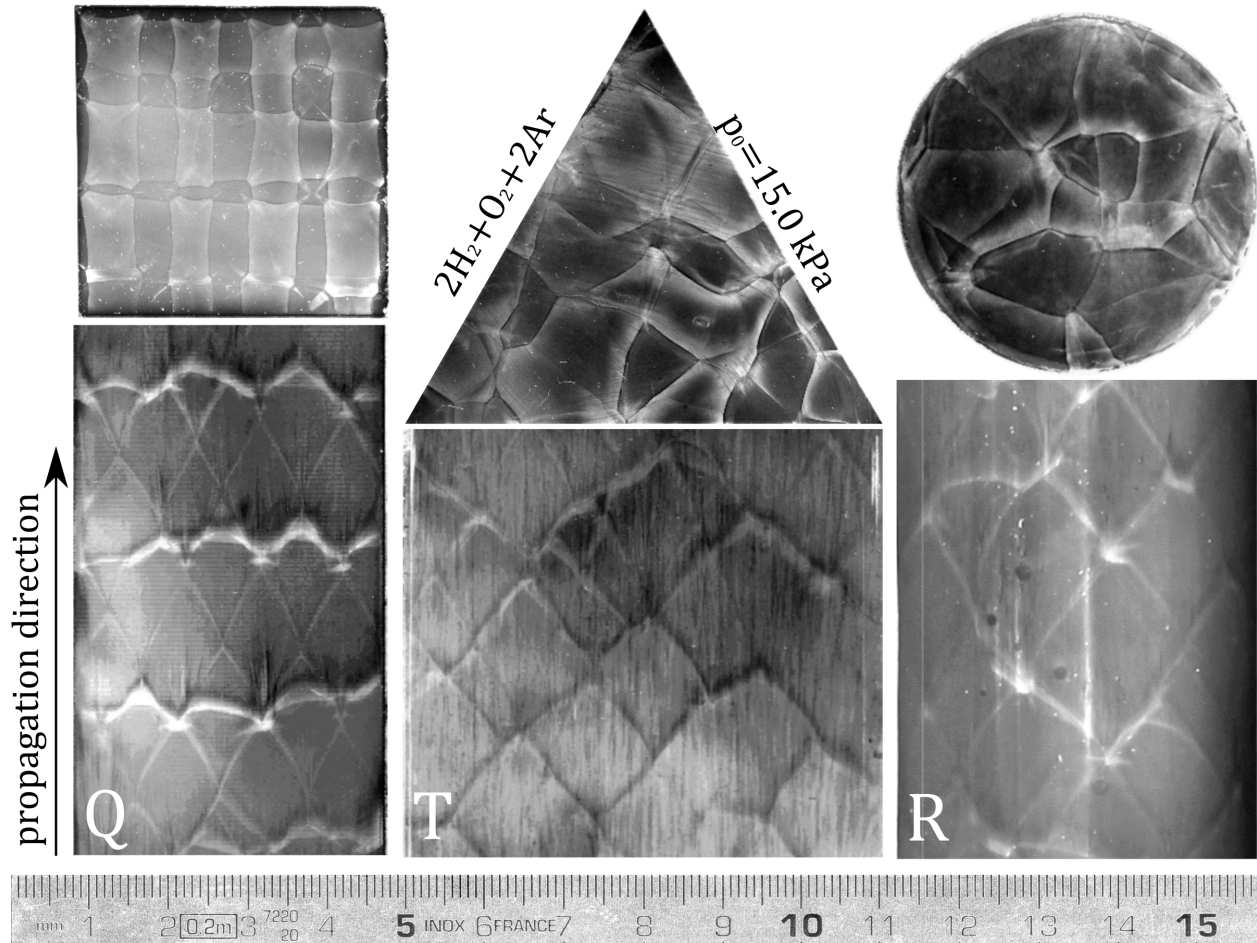


Figure 2: Head-on (top) and longitudinal (bottom) soot recordings in the mixture  $2\text{H}_2 + \text{O}_2 + 2\text{Ar}$  at  $p_0 = 15.0 \text{ kPa}$  in round (R), triangular (T) and square (Q) tubes with the same cross-section area ( $16 \text{ cm}^2$ ).

walls and no impacts of transverse fronts on the longitudinal plate anymore. The head-on patterns look the same regardless of the cross-section shape. They show the same complexity without evident local and global symmetries. The longitudinal recordings in the Q tube (Fig. 6) also look the same as in the T and R tubes, in particular, they do not show reflection impacts of the transverse fronts anymore, as they did for the lower values of  $p_0$ .

The longitudinal soot recordings point to two other observations. The first is the paradoxical result that the longitudinal patterns are regular even in the cases where the head-on patterns are not, regardless of the tube. The second is that the cells are slimmer in the Q tube than in the T and R tubes. Although perhaps limited to regular mixtures, this opposite evolution participates in raising questions about the representativeness conditions of a single length for characterizing detonation cells, at least about those deduced from longitudinal recordings alone.

Nevertheless, Figure 7 shows the cell average widths  $\lambda$  from longitudinal recordings for each cross-section shape as function of the initial pressure  $p_0$ . The widths were measured

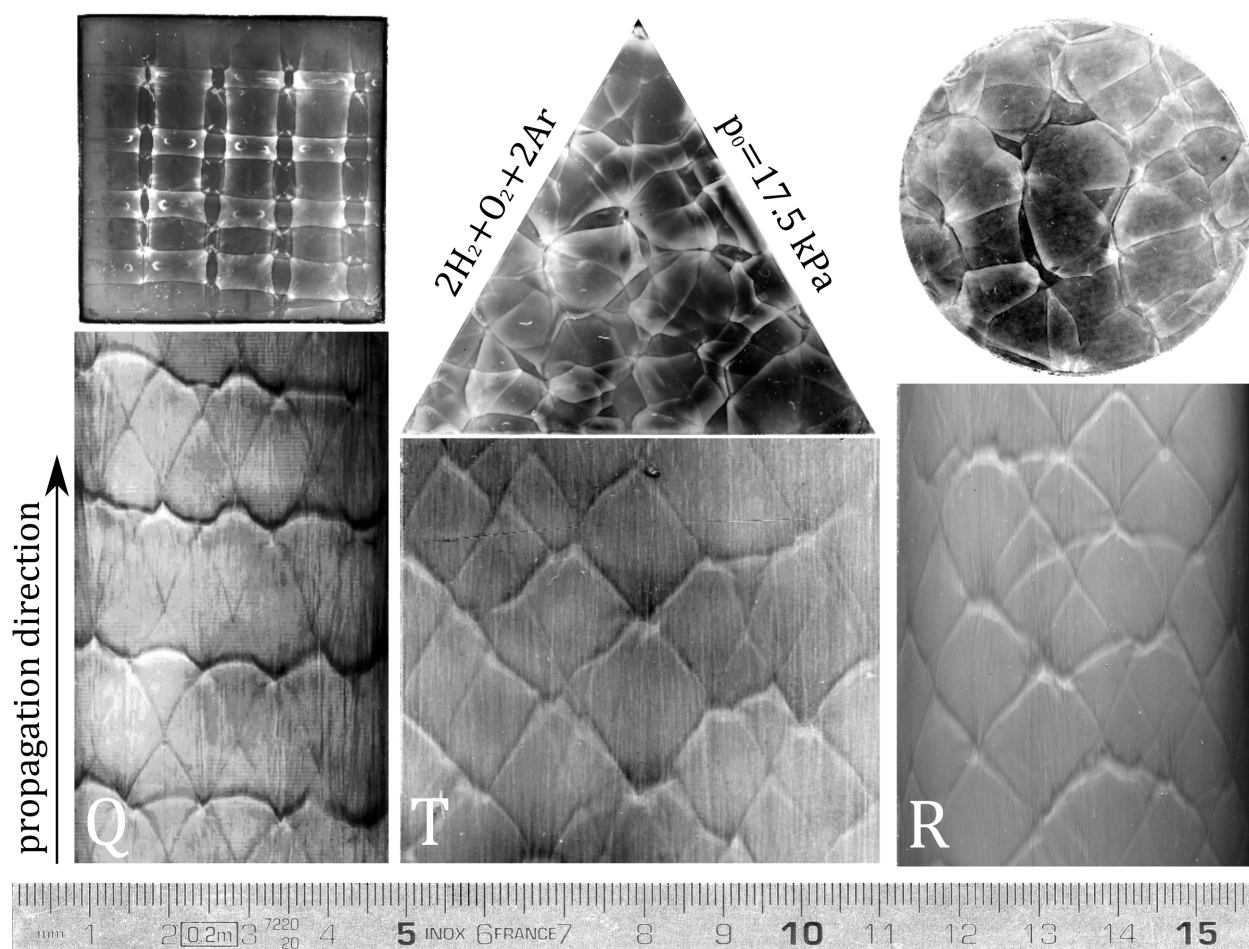


Figure 3: Head-on (top) and longitudinal (bottom) soot recordings in the mixture  $2\text{H}_2 + \text{O}_2 + 2\text{Ar}$  at  $p_0 = 17.5 \text{ kPa}$  in round (R), triangular (T) and square (Q) tubes with the same cross-section area ( $16 \text{ cm}^2$ ).



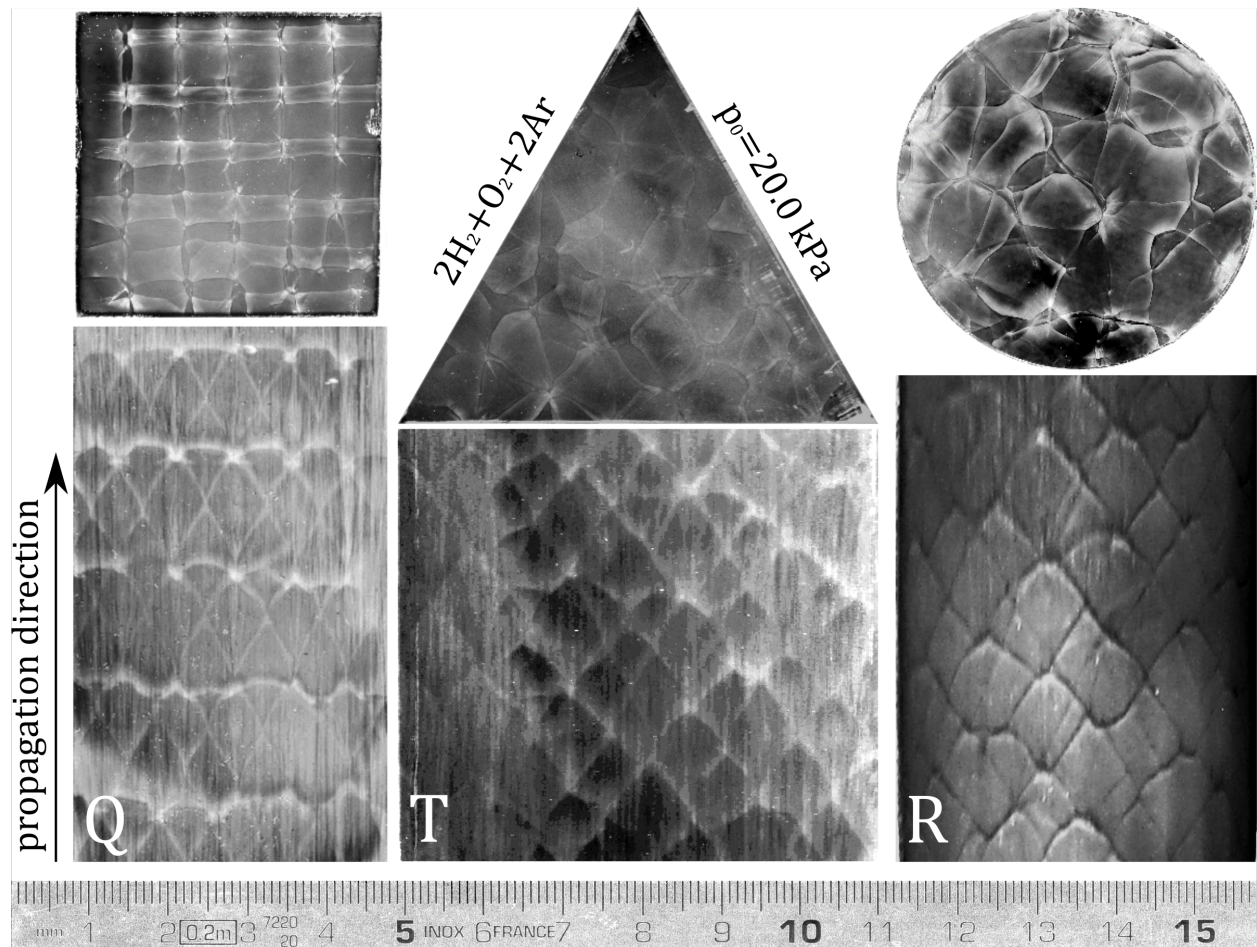


Figure 4: Head-on (top) and longitudinal (bottom) soot recordings in the mixture  $2\text{H}_2 + \text{O}_2 + 2\text{Ar}$  at  $p_0 = 20.0 \text{ kPa}$  in round (R), triangular (T) and square (Q) tubes with the same cross-section area ( $16 \text{ cm}^2$ ).

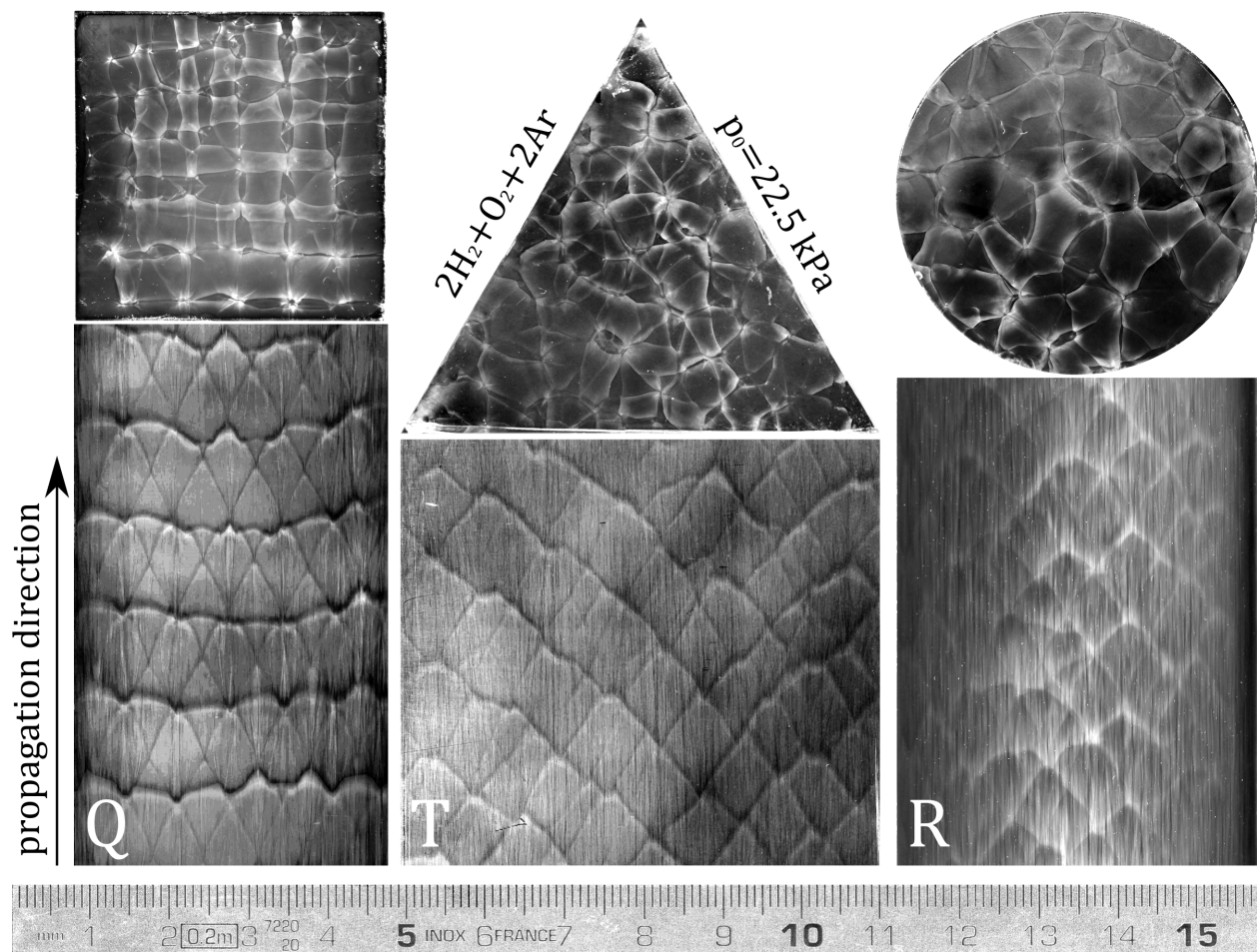


Figure 5: Head-on (top) and longitudinal (bottom) soot recordings in the mixture  $2\text{H}_2 + \text{O}_2 + 2\text{Ar}$  at  $p_0 = 22.5 \text{ kPa}$  in round (R), triangular (T) and square (Q) tubes with the same cross-section area ( $16 \text{ cm}^2$ ).

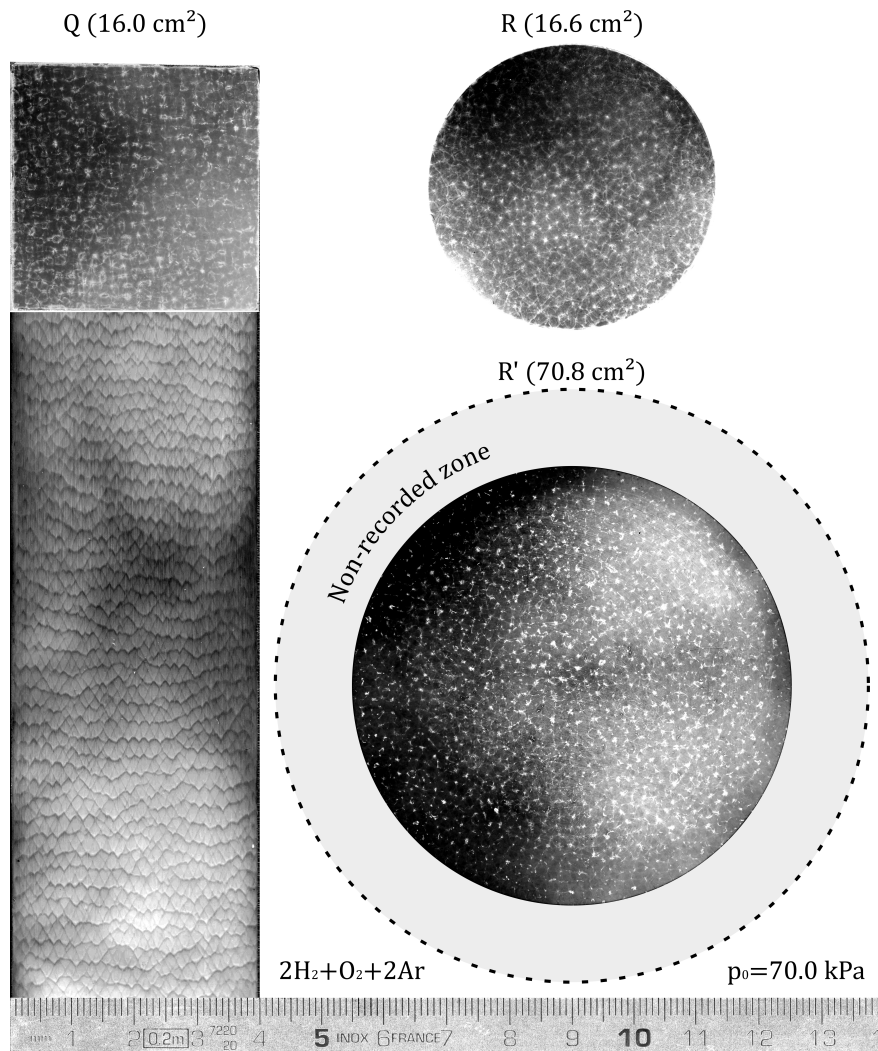


Figure 6: Head-on soot recordings in the mixture  $2\text{H}_2 + \text{O}_2 + 2\text{Ar}$  in the Q, R and R' tubes and longitudinal soot recording in the Q tube at  $p_0 = 70.0$  kPa. The periphery of the R'-tube cross-section could not be recorded.

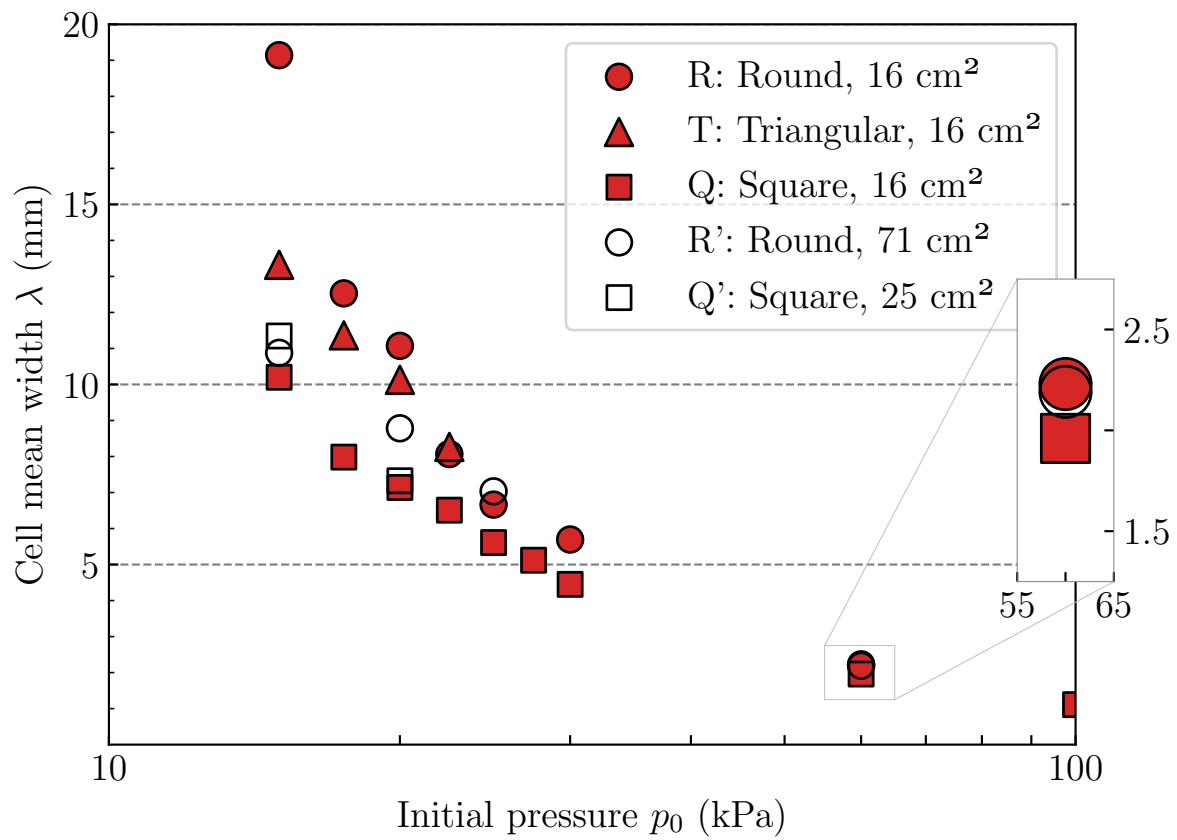


Figure 7: Cell average widths measured at the tube walls as function of the initial pressure  $p_0$  and the shape and the area of the cross section of the tubes. Measurement uncertainty is about the same as the marker heights.

classically on the longitudinal soot recordings as the distances between two transverse waves projected normal to the average incident shock direction [25, 29]. Their averaging includes at least 50 measurements along each recording, and the resulting uncertainty is approximately the size of the coordinate markers in the figure.

These averages show the usual decreasing trend with increasing  $p_0$  regardless of the cross-section shape and, if  $p_0 > 25.0\text{--}30$  kPa, they meet the well-known empirical relation  $\lambda \propto p_0^{-\alpha}$  with  $1.1 < \alpha < 1.3$ , e.g., [61]. Their differences from one shape to another increase with decreasing  $p_0$ . The difference from the Q to the R shapes increases progressively with  $p_0$  decreasing from 20.0 kPa whereas that from the T to the R shape is more abrupt at  $p_0$  about 15.0 kPa. The cell widths in the R tube are the larger, those in the Q tube the smaller. Their differences can be as large as  $\sim 100\%$  for the lower initial pressure  $p_0 = 15$  kPa. For a given  $p_0$ , the differences are small for the tubes whose cross sections have the same shape and different areas.

There are two possible interpretations. The first one is a transverse acoustics more complex in the R and T tubes that results in larger cells than in the Q tube, and the second one involves a boundary layer at the tube walls. A variation analysis in the limit of large cross sections appears not to favor the latter. For example, the basic Fay model [62, 63] reproduces at least qualitatively the increase of the boundary-layer thickness with decreasing  $p_0$ . The lower flow velocity due to viscosity in a boundary layer acts as a mass sink that induces locally a specific mass larger than in the entire cross-section. The consequences are a diverging flow and, therefore, a curvature and a velocity deficit of the average front, e.g., [64–66], that should increase with increasing thickness of the boundary layer. This description applies to cellular detonations if the cell widths are small enough compared to the transverse dimensions of the tubes so that a smooth average surface represents well the detonation front. According to Figure 7, this effect should then be more pronounced in the R tube than in the Q tube since detonation cells are larger if the shock temperature, that is, the detonation velocity, is smaller. In the limit of large cross sections, the boundary-layer thickness, denoted below by  $\delta$ , should be independent of the cross-section shapes and thin compared to the transverse dimensions of the tubes, namely here the radius  $R$  and the side  $a$  of the R and Q tubes, respectively. Their cross-section areas are  $A_R = \pi R^2$  and  $A_Q = a^2$ , those reduced by the cross-section areas of the boundary layers are  $A'_R = \pi R^2(1 - \delta/R)^2$  and  $A'_Q = a^2(1 - 2\delta/a)^2$ , so, since  $A_R = A_Q$  in this work,

$$\frac{A'_Q}{A'_R} = \left( \frac{1 - 2\varepsilon}{1 - \sqrt{\pi}\varepsilon} \right)^2, \quad (1)$$

with  $\varepsilon = \delta/a$ . This ratio is smaller than 1 for physically-small  $\delta/a$ , and decreases with increasing  $\delta/a$ . The effective cross-section area would thus be larger in a R tube than in a Q tube with the same geometric cross-section area and would decrease less rapidly in an R tube than in a Q tube. Figure 7 shows the opposite trends, that is, the cell width is larger in the R tube than in the Q tube, and the difference increases with decreasing  $p_0$ . This observation suggest that, in our conditions, possible boundary layers have a characteristic time of development larger than that of chemical-kinetics termination, which tends to favor

the hypothesis of transverse acoustic effects. Indeed, cells are still small compared to the transverse dimensions of the tubes, e.g.,  $0.05 \leq \lambda/a \leq 0.2$  ( $a = 40$  mm, Table 1) for  $p_0 \in [70, 20]$  kPa approximately, a domain where an influence of the cross-section shapes is already observed.

Another argument for acoustics is that, at lower  $p_0$ , cells are slimmer in the Q tube than in the R and T tubes, but all attain the same aspect ratio with increasing  $p_0$  regardless of the cross-section shape.

The values of  $\lambda$  become independent of the cross-section shape for all considered cross-sections areas above the same  $p_0$  for which the regularity domains disappear on the head-on recordings in the Q tube. This value of  $p_0$  is about 70.0 kPa to within the measurement uncertainty. However, although their cross-section areas are different (Table 1), the Q and Q' square tubes give similar cell widths even for the lower initial pressures. These widths agree well with those reported by Barthel [67] and Strehlow [29] (also in [68]). Below  $p_0 \leq 22.5$  kPa, the cell mean widths for the tubes with greater cross section area (Q' and R', areas 25 and 70.8 cm<sup>2</sup>, resp.) are smaller than in the T and R tubes (area 16 cm<sup>2</sup>).

It has long been observed that the closer the cell dimensions to the tube transverse dimension, the stronger the effect of the latter on the former and the detonation propagation, and that, conversely, the smaller the cells, the more independent on the tube they are and the greater the contribution of chemical kinetics compared to that of transverse acoustics, e.g. [69], p.194. For example, the increasing divergence of  $\lambda$  with decreasing  $p_0$  was noted by Strehlow and Engel [29] when they compared their measurements to those of Voitsekhovskii [45], but we could not find the tube dimensions for these experiments. Similarly, Kumar and Dewit [70, 71] noted the increasing difference between their measured and theoretical cell widths with decreasing  $p_0$ . They invoked both measurement issues and the influence of the tube size because their modelling involved only the post-shock velocity and specific-heat ratio, the initial temperature, and the induction time.

Essentially, our experiments also point out the increasing influence of the cross-section shape with decreasing initial pressure, that is, with increasing cell widths, and the difficulty to determine which minimum pressure should be considered to make sure that cells properties are dependent on chemical kinetics alone.

### *3.2. Cells patterns and phase shift in square tubes*

We carried out a detailed analysis of the detonation propagation in square-section tubes with  $p_0$  low enough so there are transverse waves moving approximately parallel to the tube walls (Subsect. 3.1). We used the grey levels on the head-on recordings to infer the propagation direction of the transverse waves, which is from the lighter to the darker domains because the latter are made up of the soot particles not swept yet by these waves (Figure 8). We thus identified two limiting modes of rectangular modes of propagation (Section 1).

Figure 9 shows a schematic, the coordinates  $x$  and  $y$  denote the transverse directions, and  $z$  the longitudinal one, i.e., that of the detonation propagation. A single longitudinal soot recording identifies the two sets of transverse waves defining a rectangular mode, one by the diamond-shaped patterns, the other by the periodic impacts of the transverse fronts

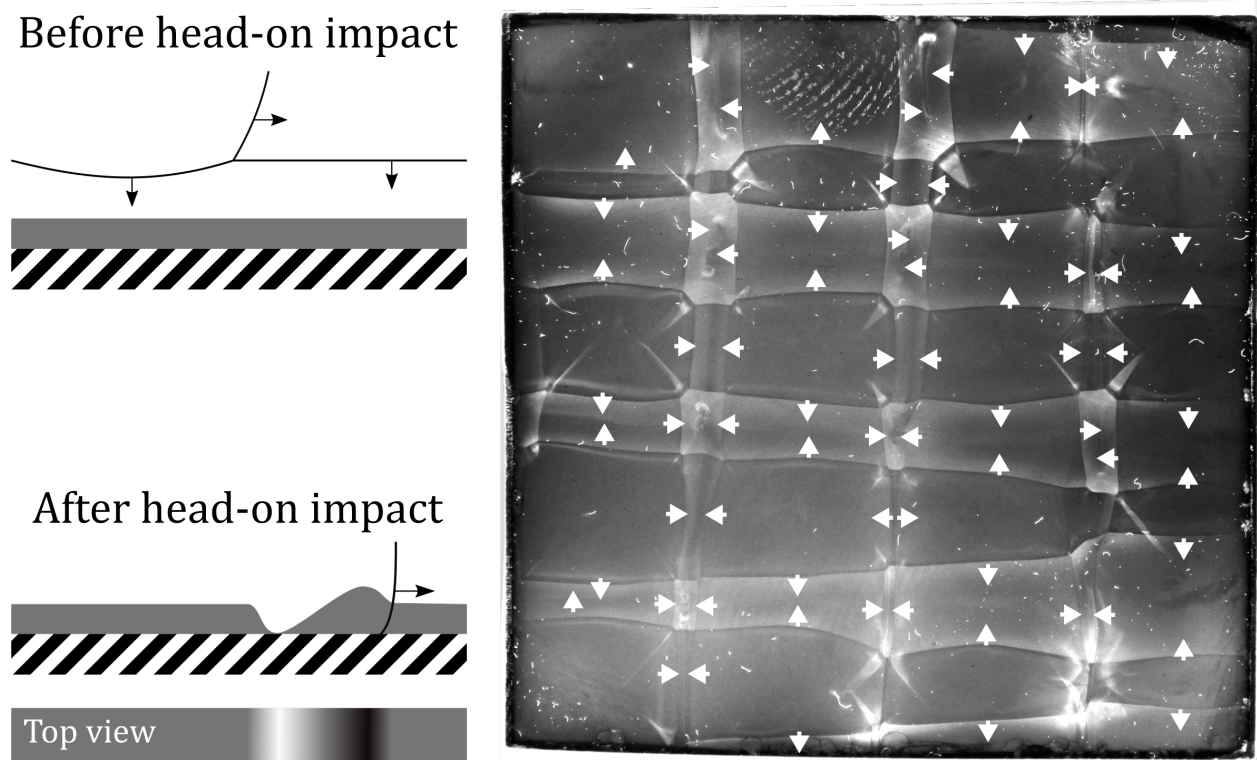


Figure 8: Left: side- and top-view schematics of the soot layer before (top) and after (bottom) the head-on impact. Right: head-on recording with the transverse-wave directions indicated by white arrow (mixture:  $\text{H}_2 + \frac{1}{2} \text{O}_2 + \text{Ar}$ ,  $p_0 = 15.0 \text{ kPa}$ , tube width  $a = 40 \text{ mm}$ )

moving about parallel to the soot plate .

It is convenient to introduce a phase shift  $\varphi$  defined as the distance between the longitudinal positions of the transverse-wave impacts in the  $x$  and  $y$  directions as schematized in Figure 9. Its minimum and maximum values are 0 and half a cell length  $\varphi_{max} = \lambda/2$ , respectively, and the value used in Figure 9 is intermediate. This definition generalizes to multi-cellular detonation regimes that introduced by Hanana et al. [39] for one-cell marginal regimes (Section 1) for which Williams et al. [55] conducted a numerical analysis with maximum value of the phase shift.

For  $\varphi = 0$ , the two sets of transverse waves are in phase, with impacts at adjacent tube walls at the same position  $z$  (Figure 10, impact position  $z_2$ ). The diagonals and the normals to the walls through the centre of the cross section are symmetry lines of the cellular front regardless of time. Each cell has a fixed center and alternates a square and a rectangular shape, which periodically grows and shrinks with an aspect ratio oscillating between 0 and  $+\infty$ .

The opposite case corresponds to transverse sets in phase opposition. The phase shift  $\varphi$  reaches its maximum value  $\varphi_{max} = \lambda/2$  (Figure 11). Similarly to the in-phase case, the cell centers have fixed positions and the square and rectangle head-on shapes alternate between each other. There is no symmetry lines any more but the head-on structure looks as though it rotates by  $\pi/2$  every time interval necessary for a longitudinal propagation be equal to  $\lambda/2$ . In Figure 11, this corresponds to the positions  $z_1$  and  $z_3$ , and  $z_2$  and  $z_4$ .

In our conditions, each longitudinal recording showed a continuous variation of the phase shift  $\varphi$  between its minimum 0 and maximum  $\lambda/2$ , e.g., Fig. 13, so the head-on recordings most often showed out-of-phase modes. Our interpretation is that the detonation propagation is subjected to long-wavelength and low-amplitude instabilities - compared to the cell dynamics - that distort the average front so its surface is warped, hence the evolutive mode of the rectangular dynamics. These instabilities might result from the ignition and system imperfections, such as an unsymmetrical shape of the wave front that comes out of the Shchelkin spiral and small defects at the tube walls. Thus, the phase and its shift are difficult to identify and measure with a practical accuracy, and appear as concepts restricted to ideal ignition system, tube and cellular detonation front, that is, neither tilted, curved, nor warped.

Another observation is that the blowup of the crossing locus of two transverse waves reveals that each splits into the same third one, although they look about normal to each other (Figure 12, red and blue lines). Each propagates partly behind, partly ahead of the other, that is, on different initial states. Therefore, their front velocities are different, which requires a third wave for their matching (green line). Regular cells in square cross-section tubes are thus bounded by two Mach stems and two incident shocks (Figure 12, states (2) and (0), resp.), so they are octagons and not rectangles. More generally, four-wave crossings on a head-on recording appear to be fortuitous with a lifetime negligible compared to the evolution time of a detonation cell.

Our analysis here points out that long-time scales phenomena affect the regularity and the symmetry of detonation cells. Numerical simulations should thus consider investigating the



propagation of cellular detonation based on initial and boundary conditions with stochastic distributions of imperfections representative of actual devices. Also, capturing the details of the transverse wave dynamics necessitates three-dimensional calculations, but whether these details significantly influences the overall detonation dynamics is an open debate.

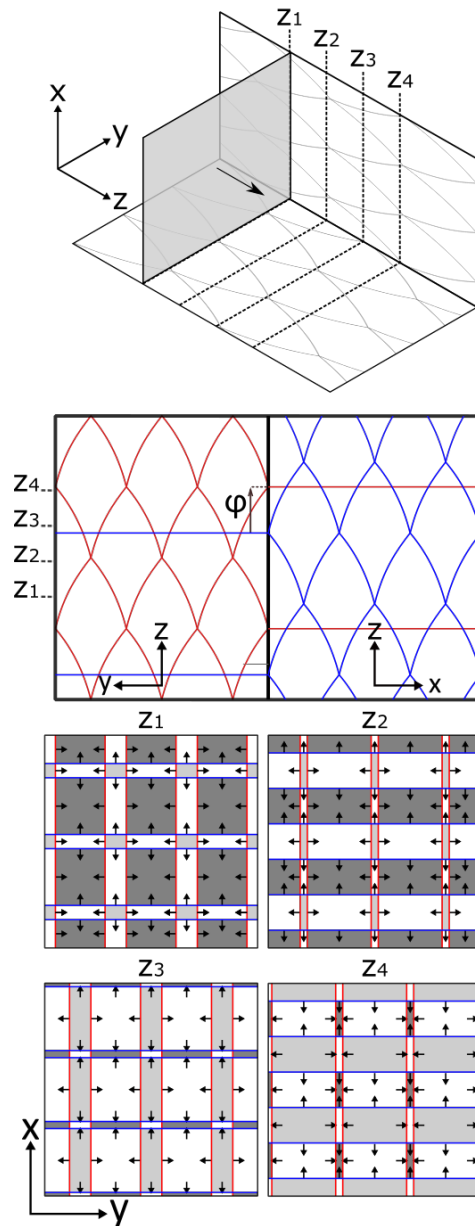


Figure 9: Schematics of the detonation cell evolution with an arbitrary phase shift  $0 < \varphi < \varphi_{max}$

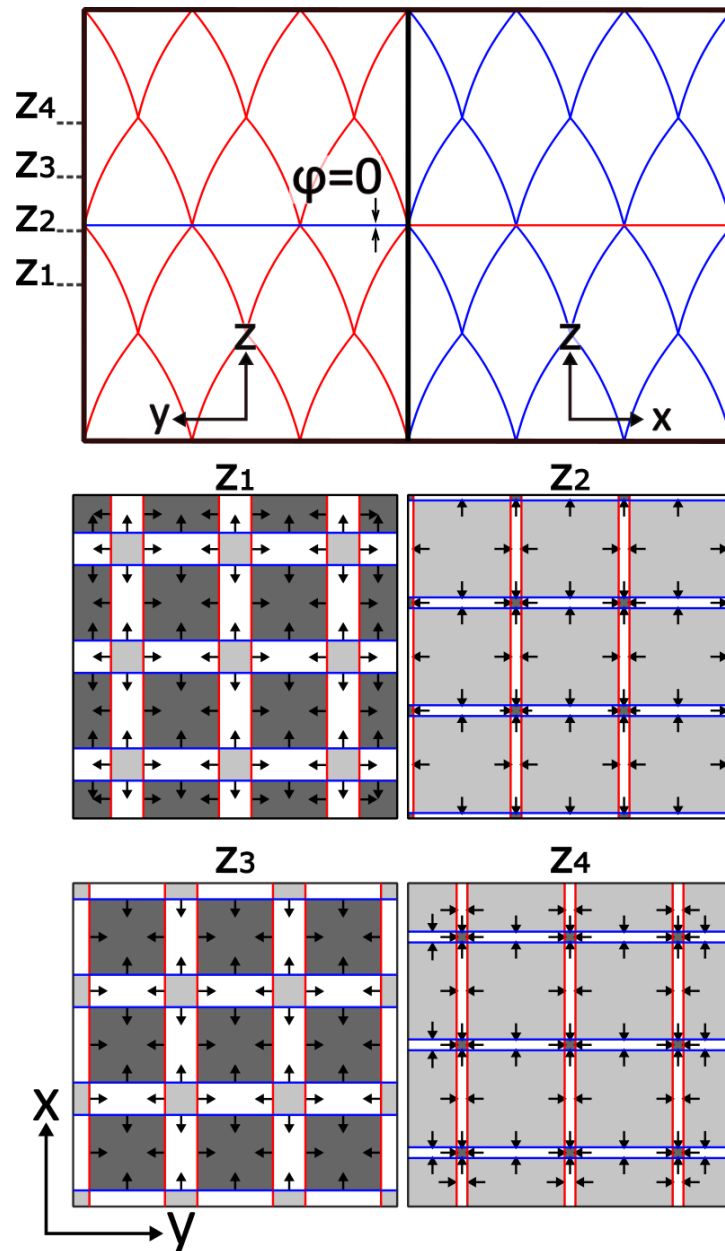


Figure 10: Schematics of the detonation cell evolution with minimum phase shift  $\varphi = 0$

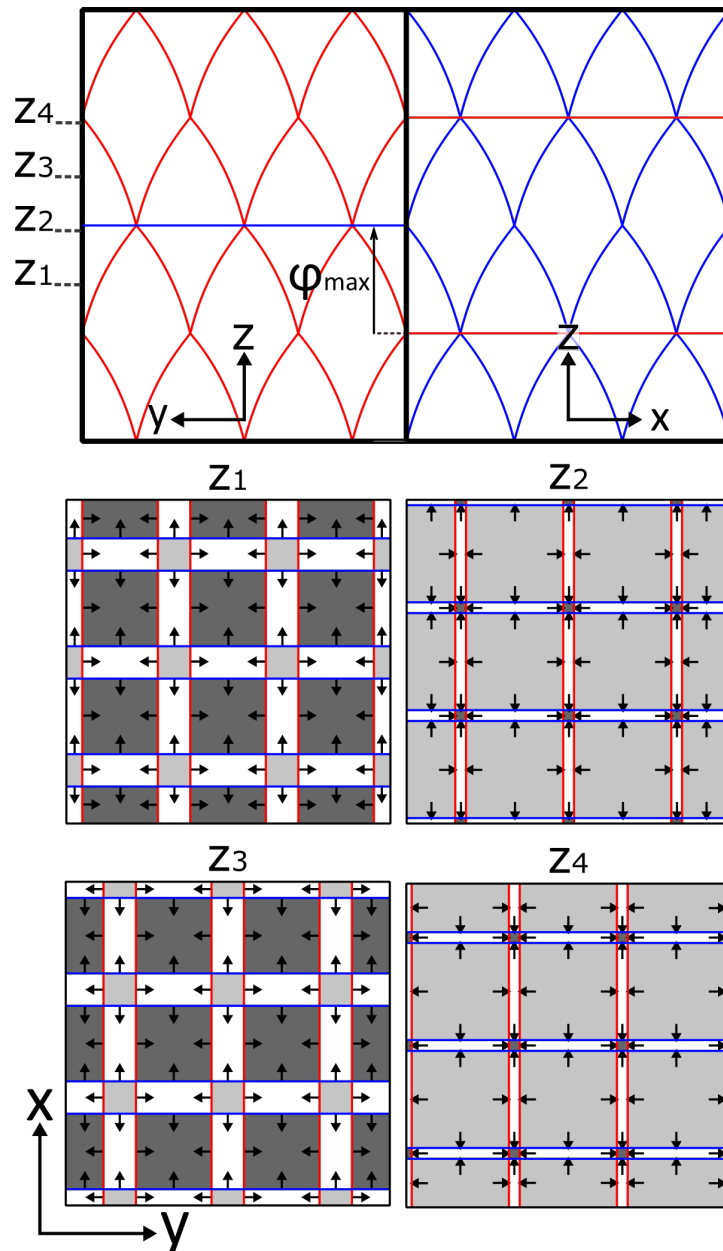


Figure 11: Schematics of the detonation cell evolution with maximum phase shift  $\varphi_{max} = \lambda/2$

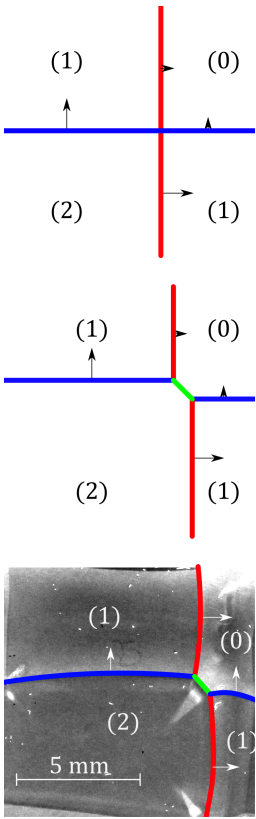


Figure 12: Blowup of crossing transverse waves

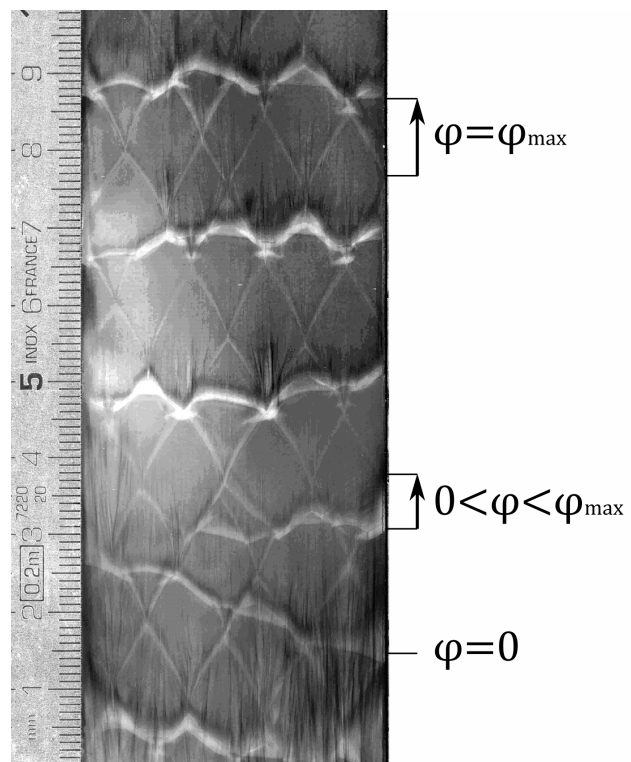


Figure 13: Example of phase shift  $\varphi$  varying from 0 to  $\varphi_{max}$  on a longitudinal soot recording for the  $2\text{H}_2 + \text{O}_2 + 2\text{Ar}$  mixture at  $p_0 = 15.0$  kPa.

#### 4. Equivalent head-on tessellation for many cells

The experimental head-on recordings indicate that the influence of the cross section shape on the cellular patterns decreases with increasing initial pressure  $p_0$  (Subsect. 3.1). Above a limiting value of  $p_0$ , the cell widths converge and their head-on patterns are irregular, that is, there is no evident periodicity in the relative positions of the cell edges. Paradoxically, the longitudinal recordings show the classical diamond-shaped regular arrangements typical of the considered mixture, both below and above the limit of influence of the cross section shape. Therefore, longitudinal recordings cannot be used alone to define an average cell width independent of the transverse acoustics. In particular, they cannot provide the limiting  $p_0$  above which transverse acoustics has no effect anymore, unless measuring cell widths in tubes with different cross-section shapes until these widths converge to the same value with increasing  $p_0$  (Figure 7).

This subsection thus discusses the definition and the representativeness of an average cell width  $\lambda$  using head-on recordings obtained in conditions presumably independent of transverse acoustics, that is, with many irregular cells. This width should be, obviously enough, of the form  $j\sqrt{A_t/F}$  where  $A_t$  is the tube cross-section,  $F$  the number of cells on the head-on recording and  $j$  an  $O(1)$  geometry factor that depends on some representative cell pattern independent of the tube. The premise here is that several head-on recordings obtained with the same composition and the same large enough  $p_0$  show the same statistical distributions of different cell patterns, e.g., triangle, square, pentagon, hexagon, etc. Equivalently, the head-on distribution, at large  $F$ , of the same pattern, is statistically independent of the impact instant of cellular fronts generated in several experiments carried out in the same conditions. Elements from graph theory and tessellation, e.g., [72] can then be used to obtain an equivalence to this pattern distribution, and hence a representative cell width.

The cells on a head-on recording can thus be viewed as a set of faces that forms a planar graph governed by the Descartes-Euler-Poincaré relation

$$V - E + F = 1, \quad (2)$$

which constrains the numbers of faces  $F$ , edges  $E$  (the transverse waves plus the intersections of the cells with the tube wall(s)), and vertices  $V$  (the intersections of transverse waves with themselves plus those with the tube wall(s)). The right-hand side of relation (2) is 2 for a convex polyhedron. The conditions that each edge is common to exactly 2 faces and each vertex to at least 3 faces give the assembly constraint

$$2E - 3V = k \geq 0, \quad (3)$$

where the integer  $k$  is the total number of edges supernumerary to 3 on a vertex, so  $k = 0$  if all vertices are common to exactly 3 edges. Combining (2) and (3) yields the average edge number per face,

$$\frac{2E}{F} = 6 \left( 1 - \frac{1}{F} \right) - \frac{2k}{F}. \quad (4)$$

In this work, the blowup of the crossing locus of transverse waves suggests that any vertex can be common to only three edges (Section 3.2). All intersects are indeed Mach configurations with three transverse waves. Therefore,  $k = 0$  here, so relation (4) for the average number of edges per face and its limit at large  $F$  reduce to

$$\frac{2E}{F} = 6 \left( 1 - \frac{1}{F} \right), \quad \lim_{F \rightarrow \infty} \frac{2E}{F} = 6. \quad (5)$$

A head-on recording with a large number of irregular cells is thus equivalent to a planar graph with the same number of hexagonal cells, that is, the hexagon is the representative pattern for cells considered as elements of a large set. The corresponding representative cell width can then be defined as the average of the inner and outer diameters of the regular hexagon, that is, of the distances between facing edges and facing vertices, respectively,

$$\lambda = \frac{6}{\pi} \int_0^{\frac{\pi}{6}} \frac{dx}{\cos x} \times d_i = \frac{3 \ln(3)}{\pi} d_i \approx 1.049 d_i, \quad (6)$$

where  $d_i = \sqrt{2A_h/\sqrt{3}}$  and  $A_h = A_t/F$  are the inner diameter and the area of the hexagon, and  $A_t$  is the cross-section area of the tube; hence,

$$\lambda = \frac{3 \ln(3)}{\pi} \sqrt{\frac{2}{\sqrt{3}} \frac{A_t}{F}} \approx 1.127 \sqrt{\frac{A_t}{F}}. \quad (7)$$

If one accepts two-wave transverse crossing, that is, four edges per vertex, such as those of head-on patterns approximated by rectangles and squares in a Q tube at low  $p_0$  (Section 3.2), the number of edges supernumerary to 3 on a vertex, per face,  $k/F$ , is 1, not 0. Relation (4) and its limit at large  $F$  then reduce to

$$\frac{2E}{F} = 4 - \frac{6}{F}, \quad \lim_{F \rightarrow \infty} \frac{2E}{F} = 4. \quad (8)$$

Here, the representation of a large number of irregular cells is a planar graph with the same number of square cells, so their width is defined by the average

$$\lambda = \frac{4}{\pi} \int_0^{\frac{\pi}{4}} \frac{dx}{\cos x} \times d_i \approx 1.122 d_i = 1.122 \sqrt{\frac{A_t}{F}}, \quad (9)$$

where  $d_i = \sqrt{A_q}$  and  $A_q = A_t/F$  are the distance between facing edges ( $a$ ) and the area of the square cell, and  $A_t$  is the cross-section area ( $a^2$ ) of the tube.

There are three observations. The first is that the average cell width for a large number of cells does not essentially depend on the actual representative cell pattern. A rough count from the recording at  $p_0 = 70$  kPa in the  $40 \times 40$ -mm<sup>2</sup> Q tube (Fig. 6) gives  $F \simeq 650$ , and relation (7) for  $F = 600, 650$  and  $700$  then gives  $\lambda = 1.84, 1.77$  and  $1.70$  mm, respectively.



These averages agree with our measurements (Fig. 7) and those of Barthel [67] and Strehlow [29] (also in [68]) although these authors do not indicate the dimensions of their tubes.

The second observation is that the sensitivity  $\Delta F/2F$  to the head-on cell number is relatively low. The cell count can indeed be difficult, depending on the quality of the head-on recordings. Relation (7) gives a relevant lower bound for measured cell widths, that is, measured values larger than the average value (7) indicate the persisting influence of transverse acoustics, to within the uncertainties.

The third observation is that relations (7) and (9) define intrinsic, minimum, uncertainties on the cell width  $\Delta\lambda/\lambda$  as the relative differences of the edge-to-edge and vertex-to-vertex distances, that is,  $1 - \sqrt{3}/2 \simeq 13.4\%$  for the hexagonal cell and  $1 - 1/\sqrt{2} \simeq 29.3\%$  for the square cell. Thus, the uncertainty is about twice smaller if the representative cell is a hexagon. However, both uncertainties are large, which questions whether a single length can characterize head-on detonation cells.

A step forward could result from the comparison in Figure 14) suggesting that a head-on view of detonation cells (left) closely resembles a Voronoi tessellation (right). A Voronoi element is the set of the closest points to a single source point in that set. Its boundaries would represent the transverse waves of the detonation front, and its source point the re-ignition locus from which these waves originated. The counting of the non-truncated Voronoi elements in Figure 14) yields  $F = 73$  faces composed of 0 triangles, 12 rectangles, 21 pentagons, 25 hexagons, 13 heptagons, and 2 octagons. The majority, 63%, are pentagons or hexagons, i.e., with 5 or 6 edges, which is consistent with the upper bound 6 indicated by the relation (5). Here indeed,  $2E/F = 5.62$ , which is close to  $6(1 - 1/F) = 5.92$ . This slight deviation

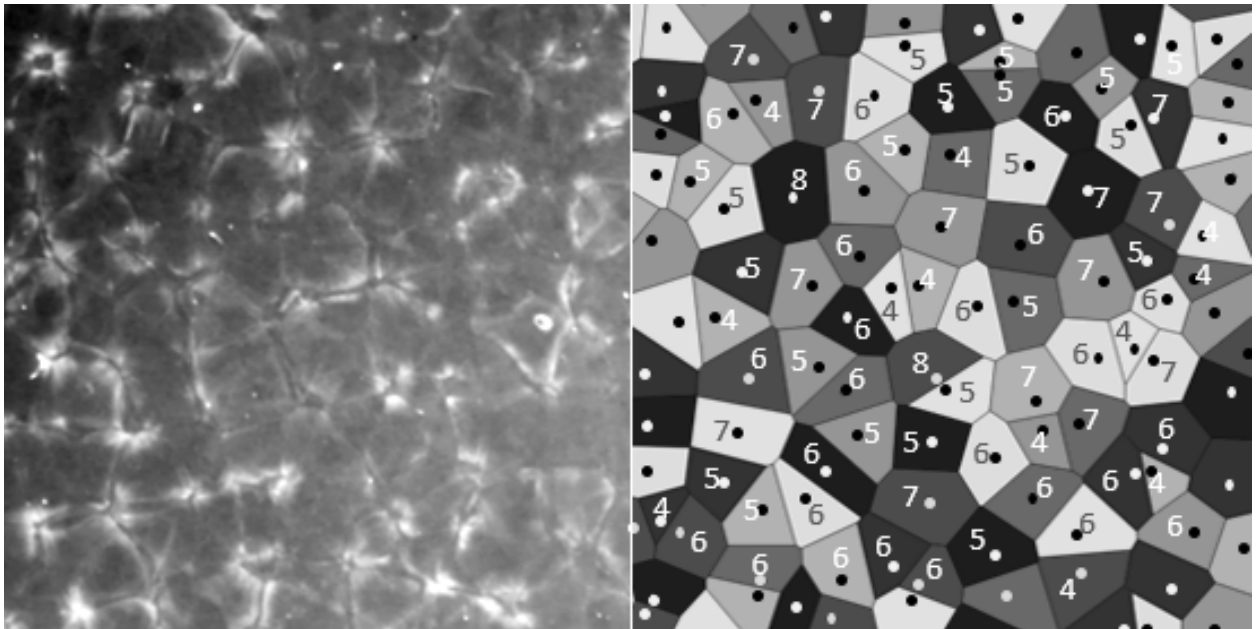


Figure 14: Head-on recording in the Q tube extracted from Figure 6(left) and Voronoi tessellation with randomly-distributed point sources (right).

may result from the number of faces  $F = 73$  not being large enough. Statistics from a tenth of other similarly-generated tessellations give about the same distribution and the same deviation, with very few or zero triangles and octagons, and only once a nonagon. In this example, the boundaries of the tessellation elements are not the contours of the detonation cells on the experimental extract because these are not defined well enough for a valuable automatic detection. Instead, we generated the Voronoi tessellation from a random distribution of sources, the number of which we chose so that the elements had similar dimensions to the experimental extract. This tessellation technique thus represents a mathematical model for the head-on view of a cellular detonation suited to alternate modelling such as a cellular automaton. As it stands, however, a supplementation with a physical criterion is necessary to predict the number of source points per unit front surface.

## 5. Discussion and conclusions

The results above aim at providing an experimental basis for revisiting the notions of regularity and characteristic width for detonation cells. We implemented the soot-plate technique to record head-on and longitudinal traces of the cellular structure of the detonation front in the mixture  $2\text{H}_2 + \text{O}_2 + 2\text{Ar}$  at the initial temperature  $T_0 = 294\text{ K}$  and the initial pressure  $p_0$  varying from 15 kPa to 100 kPa (Sect. 2). This mixture is termed stable because its detonation cells in a tube with a square or a rectangular cross-section show regular diamond-shaped patterns on longitudinal recordings and, for low-enough  $p_0$ , alternate square and rectangular patterns on head-on recordings. In this study, we analyzed its cellular dynamics in detonation tubes whose cross sections have the same surface area but different shapes, namely square, triangular and round (Sect. 3).

This work addressed only the case of the mixture  $2\text{H}_2 + \text{O}_2 + 2\text{Ar}$ , for which exists conditions on geometry and chemical kinetics for observing regularity. Therefore, a similar investigation is necessary to understand the cellular dynamics of irregular mixtures such as heavy fuels diluted with nitrogen, depending on the cross-section shape of the tubes.

The distinction between regular and irregular cells or between stable and unstable mixtures relies essentially on longitudinal recordings in square-section tubes. However, we found that longitudinal and head-on recordings do not define the same regularity. Whereas the cell patterns on the longitudinal recordings are regular for all considered  $p_0$  and cross-section shapes, those on the head-on recordings are irregular except for the square shape and low-enough  $p_0$  (Subsect. 3.1). Therefore, the cellular dynamics at the walls of a tube is not representative of that on the whole detonation front, and longitudinal soot traces alone are not sufficient for describing the cellular structure.

We presented geometrical elements from graph theory suggesting that a tessellation of regular hexagons can model a large set of irregular cells on a head-on recording (Sect. 4). The analysis indicates that a large number of cells is necessary for characterizing cells by a single length, and then defines a cell average width  $\lambda$  and its intrinsic minimum error  $\Delta\lambda/\lambda \simeq 13.4\%$ . This large value emphasizes the difficulty for numerical simulation to represent a detonation front with many cells, essentially the right balance between numerical

accuracy and physical representativeness of the chemical kinetics. For example, considering the simplest global Arrhenius rate and denoting  $E_a$  the activation energy,  $R$  the universal gas constant and  $T_H$  the shock temperature, we have  $\lambda \propto \exp(E_a/RT_H)$  in the limit of large reduced activation energy  $E_a/RT_H$ , hence

$$\frac{\Delta E_a}{E_a} = \frac{RT_H}{E_a} \frac{\Delta \lambda}{\lambda}. \quad (10)$$

The typical values  $T_H = 1500$  K and  $E_a = 20$  kcal/mole, with molecular mass  $M = 20 \times 10^{-3}$  kg/mole,  $R = 8.314$  J/mole/K, and  $\Delta \lambda/\lambda \simeq 0.1$  then gives  $\Delta E_a/E_a \approx 0.3\%$ . This small number implies that values of  $E_a$  can always be found for satisfactory restitution of a single characteristic length such as  $\lambda$ , although this Arrhenius rate cannot often represent the actual kinetics. The physical interpretation is that both a detailed scheme of chemical kinetics and more advanced conceptual tools than a single length are necessary for characterizing detonation cells.

Our analysis also points out that phenomena with characteristic times at least the effective reaction time can modulate the regularity and the symmetry of detonation cells (Subsect. 3.2). The simulation of cellular detonations should thus also include initial and boundary with stochastic distributions of defects representative of actual devices. Today, this simulation relies essentially on Euler's equations for compressible reactive fluids. However, the uncertainties in the numerical technique, the chemical kinetics, the equations of state, the multi-physics of interface phenomena, and hence the still very long computation times for three-dimensional waves do not make the physical interpretation of the computations less uneasy and time-consuming than that of the experiments.

Simplified partial differential equations with the same mathematical hyperbolic structure as Euler's, such as Burger's with a non-viscous source term, are modelling substitutes helpful to understand detonation instabilities and structures, e.g., [73–76]. Combining simulation and modelling with applied mathematics tools on pattern generation and arrangements, such as information entropy and Voronoi tessellations, e.g., [72], could bring detonation cell analysis closer to the mathematical corpus of dynamical systems and help to better characterize distributions with several cell patterns (Sect. 4).

## **Acknowledgements**

This work was supported by Région Nouvelle Aquitaine.

## References

- [1] Y. N. Denisov, Y. K. Troshin, Pulsating and spinning detonation of gaseous mixtures in tubes, *Dokl. Akad. Nauk SSSR* 125 (1959) 110–113.
- [2] C. Campbell, D. W. Woodhead, The ignition of gases by an explosion-wave. Part I. Carbon monoxide and hydrogen mixtures, *J. Chem. Soc.* 129 (1926) 3010–3021. doi:10.1039/JR9262903010.
- [3] P. Clavin, G. Searby, *Combustion Waves and Fronts in Flows: Flames, Shocks, Detonations, Ablation Fronts and Explosion of Stars*, Cambridge University Press, 2016. doi:10.1017/CB09781316162453.
- [4] A. Higgins, Steady one-dimensional detonations, in: F. Zhang (Ed.), *Shock Waves Science and Technology Library*, Vol. 6, Springer, Berlin, Heidelberg, 2012, pp. 33–105. doi:10.1007/978-3-642-22967-1\_2.
- [5] H. D. Ng, Detonation instability, in: F. Zhang (Ed.), *Shock Waves Science and Technology Library*, Vol. 6, Springer, Berlin, Heidelberg, 2012, pp. 107–212. doi:10.1007/978-3-642-22967-1\_3.
- [6] A. A. Vasil'ev, Dynamic parameters of detonation, in: F. Zhang (Ed.), *Shock Waves Science and Technology Library*, Vol. 6, Springer, Berlin, Heidelberg, 2012, pp. 213–279. doi:10.1007/978-3-642-22967-1\_4.
- [7] D. Desbordes, H.-N. Presles, Multi-scaled cellular detonation, in: F. Zhang (Ed.), *Shock Waves Science and Technology Library*, Vol. 6, Springer, Berlin, Heidelberg, 2012, pp. 281–338. doi:10.1007/978-3-642-22967-1\_5.
- [8] F. A. Bykovskii, Continuous spin detonations, *J. Propuls. Power* 22 (2006) 1204–1216. doi:10.2514/1.17656.
- [9] J. E. Shepherd, J. Kasahara, Analytical models for the thrust of a rotating detonation engine, Tech. Rep. FM2017.001, Explosion Dynamics Laboratory, California Institute of Technology Report (2017). doi:10.7907/DNVT-PY80.
- [10] P. Wolanski, *Research on detonative propulsion*, Lukasiewicz Research Network - Institute of Aviation, ISBN: 978-83-63539-45-0, 2021.
- [11] A. A. Vasil'ev, Cell size as the main geometric parameter of a multifront detonation wave, *J. Propuls. Power* 22 (2006) 1245–1260. doi:10.2514/1.20348.
- [12] R. Soloukhin, Nonstationary phenomena in gaseous detonation, *Symp. (Int.) Combust.* 12 (1) (1969) 799–807. doi:10.1016/S0082-0784(69)80461-3.

- [13] J. H. S. Lee, M. I. Radulescu, On the hydrodynamic thickness of cellular detonations, *Combust. Explos. Shock Waves* 41 (6) (2005) 745–765. doi:10.1007/s10573-005-0084-1.
- [14] M. I. Radulescu, G. J. Sharpe, C. K. Law, J. H. S. Lee, The hydrodynamic structure of unstable cellular detonations, *J. of Fluid Mech.* 580 (2007) 31–81. doi:10.1017/S0022112007005046.
- [15] S. Boulal, P. Vidal, R. Zitoun, T. Matsumoto, A. Matsuo, Experimental investigation on detonation dynamics through a reactivity sink, *Combust. Flame* 196 (2018) 11–25. doi:10.1016/j.combustflame.2018.05.017.
- [16] P. V. Tiggelen, J. Libouton, Evolution des variables chimiques et physiques à l'intérieur d'une maille de détonation, *Ann. Phys. Fr.* 14 (1989) 649 – 660. doi:10.1051/anphys:01989001406064900.
- [17] G. J. Sharpe, J. J. Quirk, Nonlinear cellular dynamics of the idealized detonation model: Regular cells, *Combust. Theor. Model.* 12 (1) (2008) 1–21. doi:10.1080/13647830701335749.
- [18] J. Shepherd, Chemical kinetics of hydrogen-air-diluent detonations, in: J.-C. Leyer, R. Soloukhin, J. Bowen (Eds.), *Dynamics of Explosions*, Vol. 106, Progress in Astronautics and Aeronautics Series, 1986, pp. 263–293. doi:10.2514/5.9781600865800.0263.0293.
- [19] D. W. Stamps, S. R. Tieszen, The influence of initial pressure and temperature on hydrogen-air-diluent detonations, *Combust. Flame* 83 (3) (1991) 353–364. doi:10.1016/0010-2180(91)90082-M.
- [20] Y. Auffret, D. Desbordes, H. Presles, Detonation structure of  $C_2H_4 - O_2 - Ar$  mixtures at elevated initial temperature, *Shock Waves* 9 (1999) 107–111. doi:10.1007/s001930050145.
- [21] Y. Auffret, D. Desbordes, H. Presles, Detonation structure and detonability of  $C_2H_2 - O_2$  mixtures at elevated initial temperature, *Shock Waves* 11 (2001) 89–96. doi:10.1007/PL00004069.
- [22] G. Ciccarelli, T. G. Ginsberg, J. L. Boccio, The influence of initial temperature on the detonability characteristics of hydrogen-air-steam mixtures, *Combust. Sci. Technol.* 128 (1-6) (1997) 181–196. doi:10.1080/00102209708935708.
- [23] A. Gavrikov, A. Efimenko, S. Dorofeev, A model for detonation cell size prediction from chemical kinetics, *Combust. Flame* 120 (1) (2000) 19–33. doi:10.1016/S0010-2180(99)00076-0.

- [24] J. Shepherd, I. Moen, S. Murray, P. Thibault, Analyses of the cellular structure of detonations, *Symp. (Int.) Combust.* 21 (1) (1988) 1649–1658. doi:10.1016/S0082-0784(88)80398-9.
- [25] H. Zhao, J. H. Lee, J. Lee, Y. Zhang, Quantitative comparison of cellular patterns of stable and unstable mixtures, *Shock Waves* 26 (10) (2016) 621–633. doi:10.1007/s00193-016-0673-9.
- [26] Y. Zhang, L. Zhou, H. Meng, T. Honghui, Reconstructing cellular surface of gaseous detonation based on artificial neural network and proper orthogonal decomposition, *Combust. Flame* 212 (2020) 156–164. doi:10.1016/j.combustflame.2019.10.031.
- [27] V. I. Manzhalei, V. V. Mitrofanov, V. A. Subbotin, Measurement of inhomogeneities of a detonation front in gas mixtures at elevated pressures, *Combust. Explos. Shock Waves* 10 (1974) 89–95. doi:10.1007/BF01463793.
- [28] R. Strehlow, R. Liaugminas, R. Watson, J. Eyman, Transverse wave structure in detonations, *Symp. (Int.) on Combust.* 11 (1) (1967) 683–692. doi:10.1016/S0082-0784(67)80194-2.
- [29] R. A. Strehlow, C. D. Engel, Transverse Waves in Detonations: II. Structure and Spacing in  $\text{H}_2\text{—O}_2$ ,  $\text{C}_2\text{H}_2\text{—O}_2$ ,  $\text{C}_2\text{H}_4\text{—O}_2$ , and  $\text{CH}_4\text{—O}_2$  Systems, *AIAA J.* 7 (8) (1969) 492–496.
- [30] V. I. Manzhalei, V. A. Subbotin, Stability of an overcompressed gas detonation, *Combust. Explos. Shock Waves* 12 (1976) 819–825. doi:10.1007/BF00740759.
- [31] V. I. Manzhalei, Fine structure of the leading front of a gas detonation, *Combust. Explos. Shock Waves* 13 (1977) 402–404. doi:10.1007/BF00740325.
- [32] I. O. Moen, G. O. Thomas, D. Bjerketvedt, P. A. Thibault, Influence of Cellular Regularity on the Behavior of Gaseous Detonations, Vol. 104, *Progress in Astronautics and Aeronautics*, 1986, Ch. III. Detonation Structure and Limit Propagation, pp. 220–243. doi:10.2514/5.9781600865800.0220.0243.
- [33] C. Paillard, G. Dupré, H. A. Aiteh, S. Youssefi-Stitou, Influence de la cinétique chimique sur la structure des détonations : cas du bioxyde de chlore, in: *Ann. Phys. Fr.*, EDP Sciences, 1989, pp. 641 – 648. doi:10.1051/anphys:01989001406064100.
- [34] P. V. Tiggelen, J. Libouton, Evolution des variables chimiques et physiques à l’intérieur d’une maille de détonation, *Ann. Phys. Fr.* 14 (6) (1989) 649–660. doi:10.1051/anphys:01989001406064900.
- [35] J. Austin, F. Pintgen, J. Shepherd, Reaction zones in highly unstable detonations, *Proc. Combust. Inst.* 30 (2) (2005) 1849–1857. doi:10.1016/j.proci.2004.08.157.

- [36] S. I. Jackson, M. Short, The influence of the cellular instability on lead shock evolution in weakly unstable detonation, *Combust. Flame* 160 (10) (2013) 2260–2274. doi:10.1016/j.combustflame.2013.04.028.
- [37] M. Short, G. J. Sharpe, Pulsating instability of detonations with a two-step chain-branching reaction model: theory and numerics, *Combust. Theor. Model.* 7 (2) (2003) 401–416. doi:10.1088/1364-7830/7/2/311.
- [38] M. Radulescu, G. Sharpe, D. Bradley, A universal parameter quantifying explosion hazards, detonability and hot spot formation:  $\chi$  number, in: D. Bradley, G. Makhviladze, V. Molkov, P. Sunderland, F. Tamanini (Eds.), *Proceedings of the 7<sup>th</sup> International Seminar on Fire and Explosion, Hazards*, Research Publishing, 2013, pp. 617–626. doi:10.3850/978-981-07-5936-0\_10-01.
- [39] M. Hanana, M. H. Lefebvre, P. J. Van Tiggelen, On rectangular and diagonal three-dimensional structures of detonation waves, in: G. Roy, S. Frolov, K. Kailasanath, N. Smirnov (Eds.), *Gaseous and Heterogeneous Detonations: Science to Applications*, ENAS Publishers, 1998, pp. 121–129.
- [40] N. Manson, Sur la structure des ondes explosives dites hélicoidales dans les mélanges gazeux, *C. R. Hebd. Scéances Acad. Sci.* 222 (1946) 46–50.
- [41] J. A. Fay, A mechanical theory of spinning detonation, *J. Chem. Phys.* 20 (6) (1952) 942–950. doi:10.1063/1.1700655.
- [42] J. Dove, H. Wagner, A photographic investigation of the mechanism of spinning detonation, *Symp. (Int.) on Combust.* 8 (1) (1961) 589–600. doi:10.1016/S0082-0784(06)80550-3.
- [43] G. L. Schott, Observations of the structure of spinning detonation, *Phys. Fluids* 8 (5) (1965) 850–865. doi:10.1063/1.1761328.
- [44] A. Macpherson, The three-dimensional wave system of spinning detonation, *Symp. (Int.) Combust.* 12 (1) (1969) 839–850. doi:10.1016/S0082-0784(69)80465-0.
- [45] B. Voitsekhovskii, V. Mitrofanov, M. Topchian, Investigation of the structure of detonation waves in gases, *Symp. (Int.) Combust.* 12 (1) (1969) 829–837. doi:10.1016/S0082-0784(69)80464-9.
- [46] R. A. Strehlow, Multi-dimensional detonation wave structure, *Astronautica Acta.* 15 (5-6) (1970) 345–357.
- [47] M. Hanana, M. H. Lefebvre, P. J. Van Tiggelen, Pressure profiles in detonation cells with rectangular and diagonal structures, *Shock Waves* 11 (2001) 77–88. doi:10.1007/PL00004068.

- [48] R. A. Strehlow, Gas phase detonations: Recent developments, *Combust. Flame* 12 (2) (1968) 81–101. doi:10.1016/0010-2180(68)90083-7.
- [49] N. Tsuboi, S. Katoh, A. K. Hayashi, Three-dimensional numerical simulation for hydrogen/air detonation: Rectangular and diagonal structures, *Proc. Combust. Inst.* 29 (2002) 2783–2788. doi:10.1016/S1540-7489(02)80339-X.
- [50] K. Eto, N. Tsuboi, A. K. Hayashi, Numerical study on three-dimensional c-j detonation waves: detailed propagating mechanism and existence of oh radical, *Proc. Combust. Inst.* 30 (2) (2005) 1907–1913. doi:10.1016/j.proci.2004.08.169.
- [51] R. Deiterding, Numerical structure analysis of regular hydrogen-oxygen detonations, *Proc. of Fall 2003 Meeting of Western States Section of The Combustion Institute Fall*. URL <https://resolver.caltech.edu/CaltechCACR:2003.210>
- [52] C. Wang, C.-W. Shu, W. Han, J. Ning, High resolution WENO simulation of 3D detonation waves, *Combust. Flame* 160 (2) (2013) 447–462. doi:10.1016/j.combustflame.2012.10.002.
- [53] S. Borisov, A. Kudryavtsev, Investigation of cellular detonation structure formation via linear stability theory and 2D and 3D numerical simulations, in: *Proceedings of the XXV Conference on High-Energy Processes in Condensed Matter*, Vol. 1893, AIP Conf. Proc., 2017, pp. 1–11. doi:10.1063/1.5007500.
- [54] S. Taileb, M. Reynaud, A. Chinnayya, F. Viro, P. Bauer, Numerical study of 3d gaseous detonations in a square channel., *Aerotec. Missili Spaz.* 97 (2018) 96–102. doi:10.1007/BF03405804.
- [55] D. N. Williams, L. Bauwens, E. S. Oran, Detailed structure and propagation of three-dimensional detonations, *Symposium (Int.) on Combustion* 26 (2) (1996) 2991–2998. doi:10.1016/S0082-0784(96)80142-1.
- [56] V. Deledicque, M. V. Papalexandris, Computational study of three-dimensional gaseous detonation structures, *Combust. Flame* 144 (4) (2006) 821–837. doi:10.1016/j.combustflame.2005.09.009.
- [57] H.-S. Dou, H. M. Tsai, B. C. Khoo, J. Qiu, Simulations of detonation wave propagation in rectangular ducts using a three-dimensional WENO scheme, *Combust. Flame* 154 (4) (2008) 644–659. doi:10.1016/j.combustflame.2008.06.013.
- [58] L. He, J. H. S. Lee, The dynamical limit of one-dimensional detonations, *Phys. Fluids* 7 (5) (1995) 1151–1158. doi:doi.org/10.1063/1.868556.
- [59] R. Takai, K. Yoneda, T. Hikita, Study of detonation wave structure, *Symp. (Int.) Combust.* 15 (1) (1975) 69–78. doi:10.1016/S0082-0784(75)80285-2.



- [60] H. Presles, D. Desbordes, P. Bauer, An optical method for the study of the detonation front structure in gaseous explosive mixtures, *Combust. Flame* 70 (2) (1987) 207–213. doi:10.1016/0010-2180(87)90079-4.
- [61] K. I. Shchelkin, Y. K. Troshin, Gasdynamics of combustion, Tech. Rep. NASA-TT-F-231, National Aeronautics and Space Administration (1964).
- [62] J. A. Fay, Gas phase detonations: Recent developments, *Phys. Fluids* 2 (3) (1959) 283–289. doi:10.1063/1.1705924.
- [63] Y. Gao, B. Zhang, H. D. Ng, J. H. Lee, An experimental investigation of detonation limits in hydrogen–oxygen–argon mixtures, *Int. J. of Hydrogen Energy* 41 (14) (2016) 6076–6083. doi:10.1016/j.ijhydene.2016.02.130.
- [64] W. W. Wood, J. G. Kirkwood, Diameter effect in condensed explosives. the relation between velocity and radius of curvature of the detonation wave, *J. Chem. Phys.* 22 (1954) 1920–1924. doi:10.1063/1.1739940.
- [65] J. B. Bdzil, Steady-state two-dimensional detonation, *J. Fluid Mech.* 108 (1981) 195–226. doi:10.1017/S0022112081002085.
- [66] M. Chiquete, M. Short, Characteristic path analysis of confinement influence on steady two-dimensional detonation propagation, *J. Fluid Mech.* 863 (2019) 789–816. doi:10.1017/jfm.2018.995.
- [67] H. Barthel, Predicted spacings in hydrogen-oxygen-argon detonations, *Phys. Fluids* 17 (1974) 1547–1553. doi:10.1063/1.1694932.
- [68] M. Kaneshige, J. Shepherd, Detonation database, California Institute of Technology; Online available; accessed march 2022 (2002).  
URL [https://shepherd.caltech.edu/detn\\_db/html/H2-0x4.html](https://shepherd.caltech.edu/detn_db/html/H2-0x4.html)
- [69] J. H. S. Lee, *The Detonation Phenomenon*, Cambridge University Press, 2008, Ch. 6, p. 147–203. doi:10.1017/CB09780511754708.007.
- [70] R. K. Kumar, W. A. Dewit, Detonation cell widths in hydrogen/oxygen/diluent mixtures at low initial pressures, *J. Energy Resour. Technol.* 117 (1) (1995) 13–17. doi:10.1115/1.2835313.
- [71] R. K. Kumar, Detonation cell widths in hydrogen/oxygen/diluent mixtures at low initial pressures, *Combust. Flame* 80 (1990) 157–169. doi:10.1016/0010-2180(90)90124-A.
- [72] F. Aurenhammer, R. Klein, Voronoi diagrams, in: J.-R. Sack, J. Urrutia (Eds.), *Handbook of Computational Geometry*, North-Holland, Amsterdam, 2000, pp. 204–209. doi:10.1016/B978-044482537-7/50006-1.

- [73] W. Fickett, Detonation in miniature, *Am. J. Phys.* 47 (1979) 1050–1059. doi:10.1119/1.11973.
- [74] A. R. Kasimov, L. M. Faria, R. R. Rosales, Model for shock wave chaos, *Phys. Rev. Lett.* 110 (2013) 104–109. doi:10.1103/PhysRevLett.110.104104.
- [75] A. R. Kasimov, Detonation analogs revisited, *Proc. 25<sup>th</sup> Int. Coll. Dynamics Explosion Reactive Systems* (2015) paper 312.
- [76] S. Lau-Chapdelaine, M. Radulescu, Detonation model using Burgers equation and a pulsed reaction, *Proc. 27<sup>th</sup> Int. Coll. Dynamics Explosion Reactive Systems* (2019) paper 315.